Univerzita Komenského v Bratislave

Fakulta matematiky, fyziky a informatiky

Dušan Plašienka

Autoreferát dizertačnej práce

Study of structural transformations in solids by computer simulations

Ab initio molecular dynamics study of pressure-induced amorphization and polyamorphism in sulfur and carbon dioxide

na získanie akademického titulu philosophiae doctor

v odbore doktorandského štúdia: 4.1.2. Všeobecná fyzika a matematická fyzika

Bratislava 2012

Dizertačná práca bola vypracovaná v dennej forme doktorandského štúdia na Katedre experimentálnej fyziky, FMFI UK

Predkladateľ: Mgr. Dušan Plašienka
Katedre experimentálnej fyziky
Fakulta matematiky, fyziky a informatiky
Univerzita Komenského v Bratislave

Školiteľ: Doc. Ing. Roman Martoňák, DrSc.

Oponenti: Prof. RNDr. Ján Urban, DrSc.
Katedra jadrovej fyziky a biofyziky, FMFI UK

Doc. Ing. Peter Bokes, PhD.,
Ústav jadrového a fyzikálneho inžinierstva, FEI STU

Ing. Jaroslav Tóbik, PhD
Oddelenie fyziky nanoštruktúr, EÚ SAV

Obhajoba dizertačnej práce sa koná …. **.09.2012** o …..... **h**
pred komisiou pre obhajobu dizertačnej práce vymenovanou predsedom odborovej komisie Prof. RNDr. Petrom Prešnajderom, DrSc.
na Fakulte matematiky, fyziky a informatiky, Mlynská dolina F1, 842 48 Bratislava

študijný odbor: **4.1.2. Všeobecná fyzika a matematická fyzika**

Predseda odborovej komisie:
Prof. RNDr. Peter Prešnajder, DrSc.
Oddelenie teoretickej fyziky
Katedry teoretickej fyziky a didaktiky fyziky
Fakulty matematiky fyziky a informatiky UK

Publications regarding this work:

[1] - Dušan Plašienka and Roman Martoňák, "Study of pressure-induced amorphization in sulfur using *ab initio* molecular dynamics", *Physical Review B*, Vol. **85**, No. 9, 094112 (2012).

Contents

1 Introduction

In the last two decades computer simulations became one of the most powerful tools in modern science including mathematics, natural sciences, engineering, pharmacology and socio-economics. The progress in technologies brought opportunity to produce and analyze data in amounts and quality that was possible never before. Computer simulations today play an irreproducible role in physics, where they cover progress in a number of different areas ranging from nuclear and high energy physics, astrophysics and relativity, through Earth and planetary sciences and complex systems (turbulent effects in fluids, meteorology, climatology) to condensed matter, classical mechanics and statics. Beyond testing of physical models by comparison of simulated and experimental data, computer hardware is commonly and sucesfully used as a virtual laboratory to predic system behavior under conditions not reachable by available experimental techniques or for other reasons. One of the main advantages of computer simulations not shared with experiments is the information of every particle trajectory enabling to investigate complex microscopic

processes in full detail.

In condensed matter physics and related areas, computer simulations are applicable for chemical calculations, high pressure and materials research physics or planetary sciences. In condensed matter systems, cooperative particle phenomena occur and so at least from tens to hundreds particles have to be involved in simulations. Accurate calculations of atoms and molecules based on quantum theory are commonly known as *ab initio* methods and their practical implementation became feasible only in last years. Application of computer simulations is now possible to objects of all scales ranging from single atoms and molecules through clusters, nanoscale objects and surfaces to bulk systems.

Experimental high pressure science in the last decades also underwent a large progress in techniques that are now able to maintain pressures exceeding 300 GPa enabling to study materials at conditions reigning in planetary interiors. Structural parameters of investigated samples are determined from x-ray diffraction patterns and dynamical aspects from infrared and Raman spectroscopy in the *in situ* experiments, where data are collected directly under pressure. Though providing information about large number of system characteristics, experiments also meet their limits and computer simulations then represent an excellent tool for both alternative and supplemental study.

Common effects of rising pressure on materials is densification, hardening and most importantly reorganization of system components to build more dense structure in phenomenon known as pressure-induced phase transition. This phase transition might be a sharp complete reorganization of structure involving bond reconstruction process or can be diffusionless of only displacive character without break of any bonds. The former one includes true chemical reaction often accompanied by dramatic change in electromagnetic and other properties. Structural changes might happen abruptly, when a first-order phase transition takes place or continuously in a second-order transition. In amorphous systems, gradual changes in their short-range structure that cannot be assigned to a genuine phase transition along continuous number of intermediate states are also commonly observed.

Pressure-induced phase transitions and new high pressure materials are of academic as well as practical interest for more reasons. High pressure research is of principal importance in crystallography as extreme conditions provide access to large number of polymorphs. Application of high pressure research is great in geophysics, planetary and stellar dynamics, as it is possible to investigate how materials in deep cosmic object interiors behave by uncovering which materials synthesize at which pressures. Some of the high-pressure materials possess technologically important properties which is of crucial importance in materials science.

2 Theoretical perspective and Methods

In this section, I make a summary of physical problematics concerning this work and methods that were used to obtain our results. I present the basic physics of *ab initio* computer simulations used in condensed matter physics - namely density functional theory for solution of electronic problem and constant pressure molecular dynamics for solution of ionic dynamics. Next, I discuss some basic theory and open problems in the field of pressure-induced transformations leading to creation of amorphous forms, including solid-state amorphization and intriguing phenomenon of

polyamorphism. I also remark the energy landscape picture of various thermodynamics phases and review the formation of conventional glasses.

2.1 First-principles calculations in condensed matter

In most condensed matter calculations, we focus on the solution of time-independent Schrödinger equation for N electrons (coordinates $\vec{r}_i$) and ions (coordinates $\vec{R}_I$ and masses M_I). In the atomic units ($m_e = e = \hbar = 1$), the equation for the total ionic-electronic wavefunction $\Psi_{tot}(\{\vec{r}\}, \{\vec{R}\})$ is

$$\Big(T_I + T_e + V_{II} + V_{eI} + V_{ee}\Big)\Psi_{tot}(\{\vec{r}\}, \{\vec{R}\}) = E_{tot}\Psi_{tot}(\{\vec{r}\}, \{\vec{R}\}), \tag{1}$$

where kinetic and potential energy operators have standard form of Coulomb interactions. These electrostatic interactions mix all particle coordinates making the problem extremely difficult. In order to find a solution, the most standard is to use the Born-Oppenheimer approximation [2], which separates the coupled problem into electronic and ionic part. The total wavefunction is written as product of electronic wavefunction $\Psi_e(\{\vec{R}\}, \{\vec{r}\})$ and ionic wavefunction $\Psi_I(\{\vec{R}\})$, which does not depend on $\vec{r}$, leading into two separate equations referred as the electronic and ionic problem.

The electronic equation reads

$$\Big(T_e + V_{eI} + V_{ee}\Big)\Psi_{e,k}(\{\vec{R}\}, \{\vec{r}\}) = E_{e,k}(\{\vec{R}\})\Psi_{e,k}(\{\vec{R}\}, \{\vec{r}\}), \tag{2}$$

where $E_{e,k}(\vec{R})$ is energy of electrons and electron-ion interactions in a quantum state k. The ionic positions $\vec{R}$ play role of external parameters here. The remaining equation for moving ions is

$$\Big(T_I + V_{eff}(\{\vec{R}\})\Big)\,\Psi_I(\{\vec{R}\}) = E_{tot}\Psi_I(\{\vec{R}\}), \tag{3}$$

$$V_{eff}(\{\vec{R}\}) = V_{II} + E_{e,k}(\{\vec{R}\}), \tag{4}$$

and can be solved once we know the electronic solution. $V_{eff}(\{\vec{R}\})$ denotes the total effective potential felt by ions.

Electron repulsion leading to correlation effects makes eq. 2 still extremely difficult to solve and many methods of different accuracy were developed to treat it. *Ab initio* methods refer to those approximative solutions that are based on laws of quantum mechanics. Most standard chemical physics methods include Hartree-Fock (HF) and set of post-Hartree-Fock approximations, with the most accurate one being the configuration interaction. The HF method approximates electron wavefunction with a single Slater determinant thus considering exact exchange term, but no correlation effects, while post-HF methods generally take more determinants into account to treat correlation. A rather different approach is employed in the density functional theory (DFT), which uses as basic variable only electron density [3]. In DFT, exchange and correlation energy are both approximated by exchange-correlation (XC) potential being a functional of density.

2.1.1 Density functional theory and the electronic problem

DFT is method for determination of *ground-state* electron density $n_0(\vec{r})$ and energy E_0 for given ionic positions and number of electrons N. Hohenberg and Kohn [4] proved that all properties of the ground state are uniquely determined by the ground-state density, which can be found from variational principle by minimizing the appropriate energy functional.

The most common practical approach to the solution of the DFT minimization problem is based on auxiliary system of non-interacting electrons generating same ground-state density as the true interacting system [5]. The corresponding self-consistent Kohn-Sham (KS) equations for one-particle KS orbitals $\phi_{i,\sigma}(\vec{r})$ and their energies $\epsilon_{i,\sigma}$

$$\left(-\frac{1}{2}\Delta + v^{\sigma}_{KS}[n_{\uparrow}(\vec{r}), n_{\downarrow}(\vec{r})](\vec{r})\right)\phi_{i,\sigma}(\vec{r}) = \epsilon_{i,\sigma}\phi_{i,\sigma}(\vec{r}) \tag{5}$$

generate correct ground-state density of interacting system given by ground state of KS orbitals

$$n(\vec{r}) = n_{\uparrow}(\vec{r}) + n_{\downarrow}(\vec{r}) = \sum_{i,\sigma}^{N} |\phi_{i,\sigma}|^2. \tag{6}$$

The KS method describes many-electron system by effective one-particle KS potential that consists of external potential $v_{ext}(\vec{r})$, averaged potential of other electrons (Hartree potential) $u_{Hartree}[n(\vec{r})](\vec{r})$ and exchange-correlation potential $v^{\sigma}_{xc}[n_{\uparrow}(\vec{r}), n_{\downarrow}(\vec{r})](\vec{r})$ that read

$$v^{\sigma}_{KS}[n_{\uparrow}(\vec{r}), n_{\downarrow}(\vec{r})](\vec{r}) = v_{ext}(\vec{r}) + u_{Hartree}[n(\vec{r})](\vec{r}) + v^{\sigma}_{xc}[n_{\uparrow}(\vec{r}), n_{\downarrow}(\vec{r})](\vec{r}), \tag{7}$$

$$v_{ext}(\vec{r}) = -\sum_{I} \frac{Z_I}{|\vec{R}_I - \vec{r}|}, \tag{8}$$

$$u_{Hartree}[n(\vec{r})](\vec{r}) = \int \frac{n(\vec{r'})}{|\vec{r} - \vec{r'}|} d^3\vec{r'}, \tag{9}$$

$$v^{\sigma}_{xc}[n_{\uparrow}(\vec{r}), n_{\downarrow}(\vec{r})](\vec{r}) := \frac{\delta E_{xc}[n_{\uparrow}(\vec{r}), n_{\downarrow}(\vec{r})]}{\delta n_{\sigma}(\vec{r})} \tag{10}$$

with all of them being functionals of electron density that reversely depends on the orbitals. The external and Hartree potentials are in HF and DFT essentially the same and main difference is that in DFT both exchange and correlation effects are taken approximately.

The XC potential function is defined formally as functional derivative of the XC energy functional $E_{xc}[n_{\uparrow}(\vec{r}), n_{\downarrow}(\vec{r})]$ by spin density $n_{\sigma}(\vec{r})$. XC energy is defined as sum of exchange and correlation energy $E_{xc} = E_x + E_c$ and though it represents only a few percent of total energy, E_x together with E_c are responsible for chemical bonding. E_x is defined as energy difference between Hartree product and *single* Slater determinant constructed from one-particle orbitals and so is based on antisymmetrization of fermion wavefunction of spin 1/2 electrons. In the KS theory, $E_x := \langle \Phi_S | V_{ee} | \Phi_S \rangle - U[n(\vec{r})]$.

Correlation energy is defined as the entire remaining energy difference between exact energy of a proper wavefunction $|\Psi\rangle$ and total Hartree-Fock energy of a single Slater determinant (with exchange effects included) and in KS DFT is given by $E_c := \langle \Psi | T_e + V_{ee} | \Psi \rangle - \langle \Phi_S | T_e + V_{ee} | \Phi_S \rangle$.

Correlation energy holds $E_c \leq 0$ and so it plays role of solid-state physics "gluon" that binds atoms and molecules together.

Estimation of XC energy is of crucial importance in DFT, where its two parts are usually treated together by $E_{xc}[n(\vec{r})]$ functional that is estimated numerically from the known properties of homgenous electron gas (HEG) tabulated from accurate quantum Monte Carlo calculations. For slowly-varying density systems, local density approximations have been found very useful, but for general systems with more rapid density fluctuations and spin polarization, generalized gradient approximations (GGA) are used

$$E_{xc}^{GGA}[n_\uparrow(\vec{r}), n_\downarrow(\vec{r})] = \int (n_\uparrow(\vec{r}) + n_\downarrow(\vec{r})) f_{xc}[n_\uparrow(\vec{r}), n_\downarrow(\vec{r}), \vec{\nabla} n_\uparrow(\vec{r}), \vec{\nabla} n_\downarrow(\vec{r})] d^3\vec{r}, \tag{11}$$

where $f_{xc}[n_\uparrow(\vec{r}), n_\downarrow(\vec{r}), \vec{\nabla} n_\uparrow(\vec{r}), \vec{\nabla} n_\downarrow(\vec{r})]$ is an arbitrary function of spin-polarized densities and their gradients that approximate E_{xc} based on known HEG values of $\epsilon_{xc}^{\uparrow\downarrow HEG}[n_\uparrow, n_\downarrow]$ and $\partial_{n_\sigma} \epsilon_{xc}^{\uparrow\downarrow HEG}[n_\uparrow, n_\downarrow]$. Perhaps the most popular parametrization of GGA comes from the Perdew-Burke-Erzenhof (PBE) construction [6] widely used in physics and chemistry.

Almost all practical calculations of the KS equations are performed in periodic environment (including amorphous states and even isolated clusters). The KS orbitals are then written according to Bloch theorem as plane waves modified by periodic functions $u_{\vec{k}}(\vec{r})$, which can be expressed by a special plane-wave subset $e^{(\vec{k}+\vec{K}).\vec{r}}$ consisting of reciprocal $\vec{K}$ vectors. The KS orbitals are according to Born-von Karman conditions indexed by $(\vec{k}, n)$, where $\vec{k}$ is a discrete momentum point from the first Brillouin zone and n is the band index.

KS orbitals must be found iteratively by expansion in some basis set with plane-wave basis being the most widely used. Transforming the KS equations to reciprocal space gives equations for the coefficients of linear combinations $c_{\vec{k}+\vec{K},n}$ of plane waves forming each KS orbital

$$\sum_{\vec{K}'} v_{\vec{K},\vec{K}'}^{KS}(\vec{k}) c_{\vec{k}+\vec{K},n} = \epsilon_{\vec{k},n} c_{\vec{k}+\vec{K},n} \tag{12}$$

that are found by diagonalizing the $v_{\vec{K},\vec{K}'}^{KS}(\vec{k})$ matrix in the reciprocal space [7]. The number of plane waves used by computer is constrained by cutoff energy E_{cut} that together with the volume V of the simulation box (supercell) determines number of the plane waves used - $N_{pw} \sim V E_{cut}^{3/2}$, which is typically from tens to hundreds of plane waves for one KS orbital.

The KS potential (eq. 7) depends on electron density and so the KS equations must be solved iteratively until self-consistency. This requires some initial guess for density for which usually sum of single atom densities solved within the KS method with spherically symmetric potential are taken.

The plane-wave treatment of the KS equations cannot be in most practical cases applied for all electrons in the system as far as computational time to converge one electronic loop grows roughly with N^2. Fortunately, it is a common property of chemistry that electrons can be well separated to inert core electrons that behave as frozen around the nuclei and the only chemically active valence electrons. This enables to avoid full-electron calculations in *ab initio* study, but the interactions between ions and valence electrons cannot be straightforwardly addressed to the Coulomb $-Z_I/r$ potential. The problem arises from strong interaction between valence electrons and ionic centers diverging for small r leading to rapid oscillations of valence wavefunctions that

need to be described by a fairly large number of plane waves. To avoid oscillations and also to include core-valence repulsion, a description of ions by pseudopotentials (PP) is usually applied.

The concept of PP is based on separation of external ion-electron potential into Coulombic part beyond some cutoff radius and a different better-describing part below it. The most simple way how to construct an individual ionic PP is some empirical model, but more realistic is *ab initio* construction that compares true all-electron wavefunctions and wavefunctions calculated from the desired PP. One of the most important properties of PP is transferability that represents the ability of a pseudopotential to provide results with similar accuracy in various chemical environments. Widely used smooth PPs that exhibit very good transferability properties are known as Vanderbilt ultrasoft pseudopotentials [8].

There is one important technique that highly improves the plane-wave PP method by use of hybridal basis set of localized atomic orbitals and plane waves in a greater "all-electron" concept. This method is known as the projector-augmented wave (PAW) method [9] and it was developed to better describe valence electrons in the regions close to cores. Plane-wave pseudopotential method and PAW generalization are nowadays the most widely used computer implementation of the KS approach to DFT for study of solids and liquids including the most popular softwares like VASP [10] and CPMD [11], which we have used in our work on sulfur and carbon dioxide.

2.1.2 Molecular dynamics and the ionic problem

Once the electronic problem is solved in some approximation, we have immediate access to system energy characteristics, electron density, types of intra and intermolecular bonds, band structure, etc. In order to obtain other properties of system associated with behavior of ions, like structure at various conditions (phase diagrams), mechanisms of transformations, heat and electricity conduction properties, electromagnetic and superconducting properties as well as elastic constants and dynamics of lattice, further static and dynamic calculations are to be carried out.

The most natural way to investigate physical system in time is known as molecular dynamics (MD). MD is based on straightforward integration of Newton's equation of motion in a discrete manner. Practical implementation in most MD computer codes is the velocity Verlet algorithm [12] with central difference approximation for acceleration term. Initial velocities for particles are usually taken from the Maxwell-Boltzmann distribution at desired temperature.

MD can be used in classical or quantum way and even by combination of both. Classical treatment essentially means use of some classical potential model for atoms and molecules as function of positions and rotational and torsion angles (for molecules). The idea of *ab initio* MD relies on separation of ionic and electronic time scales, where ions move slowly enough to enable electrons to immediately react and adapt to current ionic positions and the adiabatic theorem is assumed to maintain that electrons remain in their actual ground state.

Forces $\vec{F}_I$ acting on ions are calculated as derivatives of the ionic effective potential V_{eff} applying the Hellman-Feynman theorem to obtain the force theorem

$$\vec{F}_I = -\frac{\partial V_{eff}(\{\vec{R}\})}{\partial \vec{R}_I} = \int n(\vec{r}) \frac{Z_I(\vec{r} - \vec{R}_I)}{|\vec{r} - \vec{R}_I|^3} d^3\vec{r} + \sum_{I,J} \frac{Z_I Z_J (\vec{R}_I - \vec{R}_J)}{|\vec{R}_I - \vec{R}_J|^3}. \tag{13}$$

Ions are then moved according to the forces like in the classical MD and so are also in *ab initio* MD treated "classically", in a sense that they always occupy sharp positions $\vec{R}_I(t)$ and not a QM state.

MS simulations of infinite (bulk) systems require use of periodic boundary conditions (PBC) applied on the simulation supercell. PBC assume a periodic array of ions moving as the calculated supercell ions and every time some ion is moved outside from the simulation box, one of its periodic images is inserted to the corresponding location. In case of small systems, where no periodicity is physically present, PBC can be applied as well by placing particles into supercell that is large enough to maintain negligible interactions between the images.

Great advantage of MD is that it essentially includes all phenomena associated with "chaotically" moving particles, like finite-temperature entropy effects, diffusion, anharmonic oscillations, etc. MD performed in a proper ensemble in principle includes all types of fluctuations and therefore chemical reactions and phase transitions are not suppressed as in static ionic calculations. Another strong feature of MD is that by generating particle trajectories, all microscopic mechanisms occurring in system can be studied in full detail.

Some of the system characteristics like ideal structure, phonon modes, equations of states (EOS) for thermodynamical quantities, elastic properties and various response functions can be studied also by static ionic calculations. To find ideal crystal structure and cell parameters at zero temperature, structural (geometric) optimization procedure is employed that leads actual system state into a nearest energy minimum. Optimizing enthalpy $H = E + PV$ instead of energy, we can find equilibrium structure also at given pressure and obtain EOS for $H(P)$ for various structures that compete in enthalpy minimization. This provides information on ideal zero-temperature phase diagram that usually quite well copies true phase boundaries at low temperatures.

Phonon modes can be found in the harmonic approximation by calculating of dynamical matrix elements coming from hessian of V_{eff}. Determination of phonon frequencies can serve several purposes, like it allows to check for mechanical stability of a given structure, uncovers molecular vibrations and rotations and types of bonds, provides general picture about typical oscillations in the system and the IR and Raman spectra can be calculated and compared to experiments. Tracking evolution of the phonon modes may also identify onset of a phase transition. Phonon spectrum also gives estimation of free energy and entropy because phonon frequencies automatically provide information on system energy levels and hence determine the partition function $Z = \sum_i \exp(-\frac{E_i}{kT})$, which further brings expressions for mean vibrational free energy $\langle F \rangle_{vib}$ and vibrational entropy S_{vib} at given temperature.

Some of other static ionic methods have also power of predicting stable crystal structures including Monte Carlo simulations, simulated annealing, minima hopping [13] and most of all the genetic algorithm [14] that is perhaps the most sucesfull method for predicting crystal structure at zero temperature available today.

Most of the world we experience every day can be in language of statistical physics well described by constant pressure-temperature (NPT) ensemble. For that reason, prediction of stable crystalline phases of material under NPT conditions is known as the crystal structure prediction (CSP) and at finite temperature [15], MD simulations present the most suitable method for solving the CSP problem. It is therefore of high interest to perform MD in NPT

environment.

As far as the Newton's equations are energy-conserving, straightforward use of MD and force theorem samples microcanonical ensemble, and so additional techniques that simulate thermostat and barostat are needed. The most used barostat that provides correct averages (but not fluctuations) is the Berendsen barostat [16]. In the anisotropic version appropriate for crystals, it works by rescaling the cell vectors $\mathbf{h} = (\vec{a}, \vec{b}, \vec{c})$, atomic positions $\vec{R}_i$ and velocities $\vec{v}_i$ by the scaling matrix $\boldsymbol{\mu}$ according to difference of predescribed external stress tensor $\boldsymbol{P}_{ext}$ and instantaneous internal stress $\boldsymbol{P}_{int}$ following

$$\mathbf{h} \to \boldsymbol{\mu}\mathbf{h}, \quad \vec{R}_i \to \boldsymbol{\mu}\vec{R}_i, \quad \vec{v}_i \to \boldsymbol{\mu}\vec{v}_i, \tag{14}$$

$$\boldsymbol{\mu} = \mathbf{1} - \frac{\beta \Delta t}{3\tau_P} \left(\boldsymbol{P}_{ext} - \boldsymbol{P}_{int} \right), \tag{15}$$

where β is bulk modulus of system, Δt is MD timestep and τ_P is relaxation time scale. We used this idea of Berendsen barostat in our simulations and implemented it to simulations performed with VASP package, which is originally written only for constant-volume simulations.

The quantum-mechanical stress tensor $\boldsymbol{P}^q_{int}$ that needs to be evaluated for barostat and other reasons can be obtained from the expression [17]

$$(\boldsymbol{P}^q_{int})^{\alpha\beta} = NkT / \langle V \rangle \, \delta^{\alpha\beta} - \frac{1}{2V} \sum_{ij} \langle \Psi | \, (\vec{r}_{ij})^{\alpha} (\vec{\nabla}_{ij} (U(r_{ij})))^{\beta} \, | \Psi \rangle \,, \tag{16}$$

where $\vec{r}_i$ and U are operators whose expectation values must be evaluated at the instantaneous quantum state $|\Psi\rangle$.

The most common problem confronted in almost all computer simulations involving larger number of particles that is especially constraining in *ab initio* simulations is the time scale problem. In first-principles calculations follows from fact that times needed to find electron density scale roughly as N^2 that enables to simulate only maximum of hundreds of picoseconds. This prevents some of the possible transitions to occur, especially when corresponding energy barriers are too high in respect to thermal fluctuations $kT \ll \Delta E$ (kinetic hindrance). The most powerful method developed to overcome this problem is the metadynamics algorithm [18].

2.2 Amorphous materials and high pressure

2.2.1 Energy landscape picture and configuration enthropy

Very instructive description of distinct system phases and transitions between them is provided by energy landscape picture [19, 20, 21, 22], which represents the potential energy surface (ES) of a system plotted on configuration space of interacting particles. ES is an extremely complicated function of high dimension that contains vast number of distinct maxima, saddle points and most important of all - local minima corresponding to local stable organizations of system components. These can be either perfect crystalline structures, but more often some polycrystallites and defective versions of crystals and also amorphous packings. Typical ES is depicted on Fig. 2.2.1 with graphical representation of different solid and liquid phases.

The global minimum (a) on ES corresponds to the most stable crystal structure C1 realized

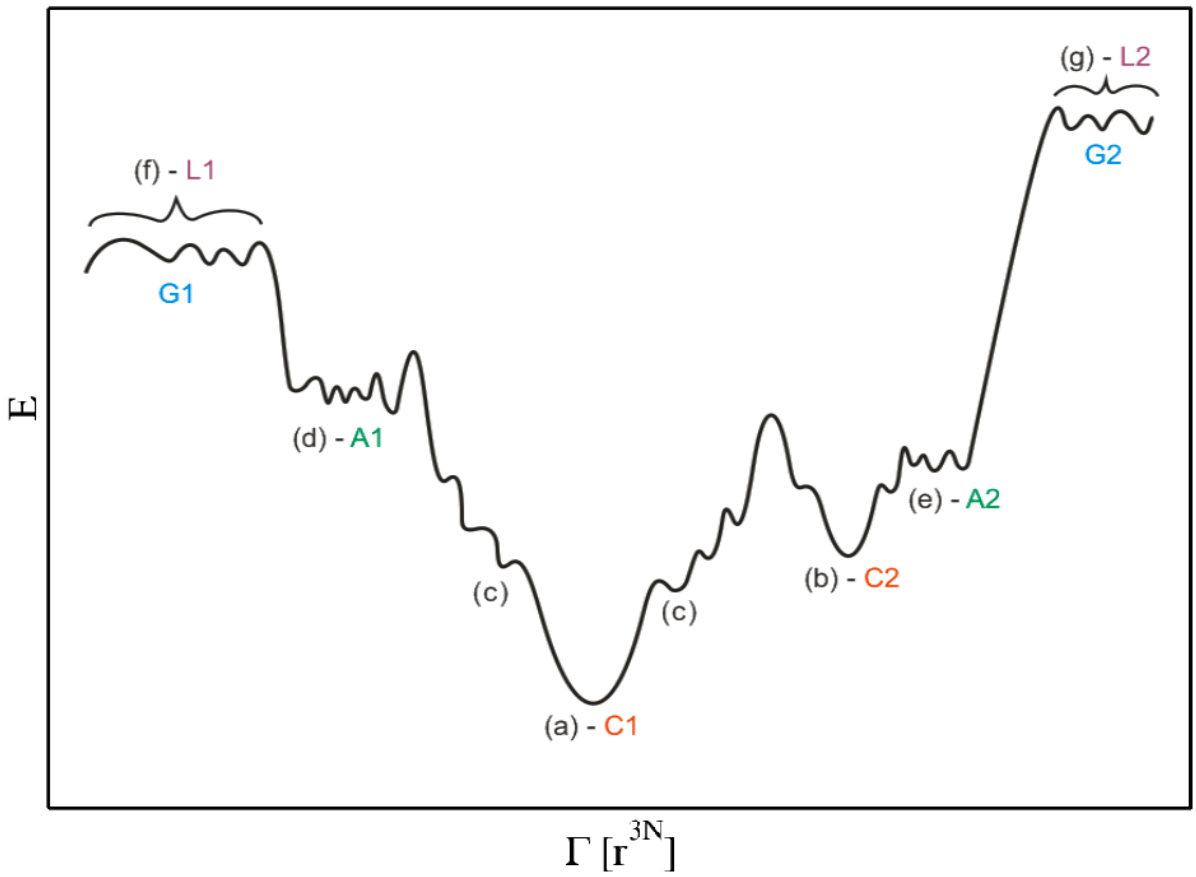

Figure 1: ES of system and its condensed phases: (a) global minimum - the most stable crystal structure C1, (b) local minimum - higher-energy crystal structure C2, (c) local minima - defective crystalline and polycrystalline packings of C1, (d) and (e) amorphous minima A1 and A2 corresponding to crystals C1 and C2, (f) liquid-like minima - liquid phase L1 and its corresponding glasses G1 and analogically (g) - L2 and G2.

at zero temperature. Another deep local minimum (b) corresponds to less stable crystal C2. Minima surrounding C1 in its basin of attraction (c) correspond to structures with presence of defects and to polycrystalline forms of the corresponding crystal. As one moves away from perfect crystalline minima, the defectiveness grows and polycrystalline scale shrinks and the minima become to correspond to amorphous packings as A1 for C1 - (d) or A2 for C2 - (e). These minima have disordered character but share some properties with their crystalline counterparts keeping same short-range order - and hence representing their amorphous versions. This can be present in shapes of radial distribution function (RDF) or values of coordination numbers, while angular distribution function (ADF) is typically much broader for amorphous forms. Amorphous phases that are connected to liquids are known as glasses - (f) and (g).

For practical reasons concerning definition of entropy of certain system state, it is suitable to split the motion of a system in two parts [20]. One is the discrete motion between adjacent local minima and second is the vibrational motion inside these minima. This idea also divides entropy of certain state into configuration and vibrational part

$$S = S_{vib} + kln(\Omega(E_{min})), \tag{17}$$

where S_{vib} is mean vibrational entropy of local minima and second term is the configuration entropy S_{conf} directly proportional to $\Omega(E_{min})$ - that is the number of local minima with same value of their minimal value - E_{min}. Concept of configuration entropy is very important for disordered states stability considerations.

2.2.2 Glasses and glass transition

Glasses are known since ancient times to form by fast cooling of melts in the phenomenon known as glass transition, which is principally based on system non-ergodicity. Starting from a liquid phase - (f) and (g) on Fig. 2.2.1 and lowering the temperature, system is directed to minimize its internal energy (or enthalpy), but as temperature falls, fluctuations also become smaller, viscosity increases [23] and if the cooling is rapid enough, system fails to find a passage leading to lower energy regions of crystalline attraction basins. As cooling continues, at some temperature - glass transition temperature T_g, supercooled liquid freezes in some high-energy minimum of a disordered state and remains trapped oscillating around some local amorphous arrangement. For that reason, not only the glass transition, but also the existence of glass phase itself is a dynamical phenomenon.

Glass transition is not a thermodynamical phase transition, because T_g as well as the exact final glassy state both depend on the cooling rate [22] as there are number of local high-energy minima of a certain megabasin that represent glass/liquid. After the glass transition is complete, the microscopic glass structure is very similar to that of the liquid phase following directly from the ES description of the glass transition. The entire process includes many effects and mechanisms still not completely understood, like dynamical heterogenity, strong and fragile glass formers, non-Arrhenius behavior, breakdown of the Stokes-Einstein equation, existence of Kauzmann temperature [24] and Kauzmann paradox (the entropy crisis), thermodynamical concept of ideal glass, rheology and aging and many more [19, 21, 22, 25, 23].

2.2.3 Pressure-induced amorphization

The most dramatic effect induced by pressure are structural transformations. Besides crystal-crystal transformation between two different polymorphs, also pressure-induced amorphization (PIA) or even amorphous-amorphous transition (AAT) are known to occur and leading to creation of phases with potentially technological interest, like amorphous semiconductors, metallic alloys or extremely hard materials.

The phenomenon of PIA (reviews [26, 27]) of a solid state as a new way to make amorphous materials was first observed in compressed ice [28] and since then was observed in a number of most common and important materials including SiO_2 [29], CO_2 [30], Si [31], S [32] or N [33]. The resulting amorphous form is known as a pressure glass - p-glass to distinguish it from quenched q-glass. Amorphization from both molecular and extended crystals were observed for all kinds of intermolecular bonding and by now, nearly a hundred compounds were reported to exhibit PIA [27]. The nature as well as mechanism of PIA have been disputed and extensively discussed since its first observation. The discussion concerns questions about thermodynamical background of PIA, connection of p-glass to crystal or liquid, exact PIA mechanism, order of the transitions, reversibility, etc.

It was recognized that PIA amorphs generally differ from quenched glasses by exhibiting some short-range crystal properties [27] and higher densities than the same P-T positioned glasses [34]. Creation of memory glasses, where PIA amorphs preserve memory of their initial crystallographic orientation were also observed - for the first time in $AlPO_4$ [35].

PIA was first associated with crossing of the low-temperature extrapolation of the metastable melting line in H_2O and then also in SiO_2 [29] and Si [31]. On the other side, in many different cases PIA occurred in the vicinity of thermodynamical crystal-crystal boundary and it was concluded that there is no systematic behavior concerning this problem [36]. The first option brought the idea of thermodynamical (cold or metastable) melting, in which system melts below its T_g transiting between two metastable phases in a first-order transition, while different model called mechanical melting is based on a catastrophic collapse of structure, which cannot withstand further change of conditions and loses stability in a spinodal decomposition.

For the mechanism of PIA, various scenarios were proposed as well. In XRD experiments, it is commonly observed that x-ray diffraction peaks become increasingly worse that indicates gradual increase of the number of defects in structures. PIA is hence often progressing around structural imperfections that play role of nucleation centers for disordering, which is usually associated with irreversible thermodynamical melting.

One of the most common model for mechanical melting is based on famous Born criteria [37] (rules for crystal stability in form of inequalities between elastic constants c_{ij}) that were originally developed to model melting, but their breakdown was observed also in the vicinity of PIA, as first predicted for SiO_2 [38] and first time directly observed in ice [36]. Another model of PIA mechanism is dynamical lattice instability associated with structural collapse due to some phonon mode softening, as first time observed in the vicinity of PIA (and of AAT as well) in compressed hexagonal ice [36]. This was often attributed to structure approaching its spinodal boundary, hence to mechanical melting scenario as well.

Mechanism of PIA is also related to some specific material type. The most typical example is case of molecular crystals, like water, carbonia, sulfur or nitrogen. In molecular crystals at low pressures, distances between molecules are much larger than bond lengths and PIA is commonly observed when large overpressurization brings them closer and the intermolecular forces become comparable to the intramolecular ones. We observed this effect in our work on PIA of sulfur as well [1]. Tetrahedral materials are another important specific category, because the building blocks of tetrahedra are unable to fill the space, but their noncrystallographic packing can reduce the volume and stabilize the amorphous form. It was also referred that compounds exhibiting negative thermal expansion often exhibit PIA [27].

The order of the PIA transition also does not exhibit a strict character, though in majority of the referred cases PIA shows many properties of first-order transitions, like large volume reduction and abrupt changes in mechanical and electrical properties. PIA was found to be reversible as well as irreversible and also strongly temperature-dependent, as far as mechanisms typical for thermodynamic melting and for mechanical melting were both observed in the same materials at different temperature - e.g. in water [39].

2.2.4 Amorphous-amorphous transition

Polyamorphism is a direct analogue to polymorphism and means that one solid substance may exist in more amorphous forms that are well-distinguishable (reviews [40, 41, 42]). Such amorphous forms differ most typically in density and great majority of polyamorphism examples refer to low density amorphous (LDA) and high density amorphous (HDA) forms. Polyamorphism was first observed also in compressed ice [43] and since then has been studied in a number of other common elements and compounds including Si [31], Ge [44], C [45], SiO_2 [46], CO_2 [30], GeO_2 [47], and many others.

The phenomenon of AAT is in much similar to PIA, including all disputation and problems concerning the thermodynamics and mechanism of the transition. The AAT was attributed to be thermodynamically connected to higher temperature low density liquid (LDL) to high density liquid (HDL) transformation and also to stable crystal-crystal transition. Accordingly, the distinct amorphous forms were considered to be connected to their corresponding liquid states or to crystalline phases.

Various amorphous forms differ in structural properties, like RDF, ADF and N_C, sometimes greatly (with different bond network - molecular and non-molecular forms), and sometimes continuously when a large number of intermediate states exists between two forms. Transitions of the former case are usually associated with a first-order phase transition, while the latter exhibit gradual changes that often cannot be associated even with a second-order transition. The most typical example of the second case is gradually changing structure with some progressively varying atomic coordination, like in case of intermediate states between fourfold tetrahedral and sixfold octahedral glass polyamorphs of GeO_2 [48] and also between three and four-coordinated solid amorphous CO_2 that we observed in our simulations.

Polyamorphism was originally associated with underlying liquid-liquid transition (LLT) in water [43] and a continuity between the stable LDL-HDL thermodynamic line and the LDA-HDA kinetic line was suggested. First simulation evidence of a stable first-order LLT was proposed to occur in liquid carbon [49] between predominantly *sp*-bonded LDL form and mostly sp^3-bonded HDL form. First empirical evidence of such transition was obtained in liquid phosphorus [50]. Sulfur has been also found to undergo a first-order LLT [51] from insulating liquid formed by S_8 molecules into a metallic liquid state of polymeric fragments proceeding *via* ring-opening polymerization [52]. Hypothesis of the LDL-HDL background process behind the AAT was most extensively studied in water (review [53]) and also in silicon [31, 54]. On the other side, LDA and HDA forms were reported to possess properties similar to low and high pressure stable crystal phases and the AAT was supposed to be a metastable analogue of crystal-crystal transformation, e.g. in sulfur [55].

AATs have been reported to proceed abruptly as well as continuously or gradually about equally often. Relatively clear evidence of first-order nature of AAT transition based on observation of sharp changes of density, structure or dynamical character were referred in H_2O [43], SiO_2 [56], Si [54], Ge [44], S [55] and CO_2 [30] and on the other side, gradual changes were observed in materials including SiO_2 [46], GeO_2 [48], C [45], etc. This second class of cases can be definitely extended also with CO_2, where our simulation results showed a continuous change in the amount of three and four-coordinated carbon atoms between fully three and four-coordinated

amorphous forms (not with the molecular to non-molecular AAT in CO_2). SiO_2 was reported both as a first-order and as a gradual-type transition and hence the role of temperature on AAT transition has been extensively discussed for SiO_2 [56] and GeO_2 [57], where a so-called pressure window was identified in which gradual and reversible changes took place and after heating a sharp transition was obtained instead.

3 Applications and results

In the following section, I summarize our simulation results on PIA and AAT observed in sulfur and carbon dioxide - simulation methods and pathways and results that are both completely new and comparative to experimental data. This includes observation of a new phase of monoclinic molecular sulfur and detailed molecular description of the amorphization mechanism published in *Physical review B* [1] and preliminary results on PIA and AAT investigation in CO_2.

3.1 Sulfur

Sulfur is one of the most common and important elements in the Universe, on Earth and in almost all life we know being one the six major biogenic elements. Sulfur is 16th element in the periodic table placed in group VIb with chemically active s^2p^4 valence shells. Sulfur at ambient conditions forms covalent molecular crystals that polymerize at rising pressure. Allotropy of sulfur at high pressures and temperatures belongs to the most complicated and interesting ones found among the pure elements and at least ten different stable crystal structures were identified.

3.1.1 Crystalline and amorphous sulfur at high pressures

The most stable crystal structure of sulfur at ambient conditions is phase S-I which is remarkebly complicated consisting out of 16 S_8 molecules (128 atoms) in the unit cell [58]. The high-pressure region of phase diagram exhibits continual densification and metallization. On pressure increase, S-I transforms to S-II and further to S-III. S-II and S-III are made of polymeric molecules of triangular and squared-shaped chains [59, 60]. At higher pressures, sulfur transforms into phase S-IV, which possesses aperiodic (incommensurate) modulation [61] and then to phase S-V with even higher pressure phases being only predicted by computer simulations [62]. Starting from the phase IV, sulfur starts to exhibit metallic and superconducting behavior [63, 64].

Molten sulfur upon rising temperature undergoes a first-order LLT λ-transition [65] leading to polymeric phase that can be quenched to glass of helical sulfuric chains. Synthesis of amorphous sulfur by PIA was reported in Ref. [32] and recently also the phenomenon of polyamorphism was observed [55]. Experiments indicated that before PIA the structure undergoes substantial changes representing progressive creation of defects or some other structural changes. The reported LDA-HDA polyamorphic transition in sulfur [55] suggested that LDA and HDA forms correspond to their crystalline counterparts, namely to polymeric S-III and extended metallic S-IV.

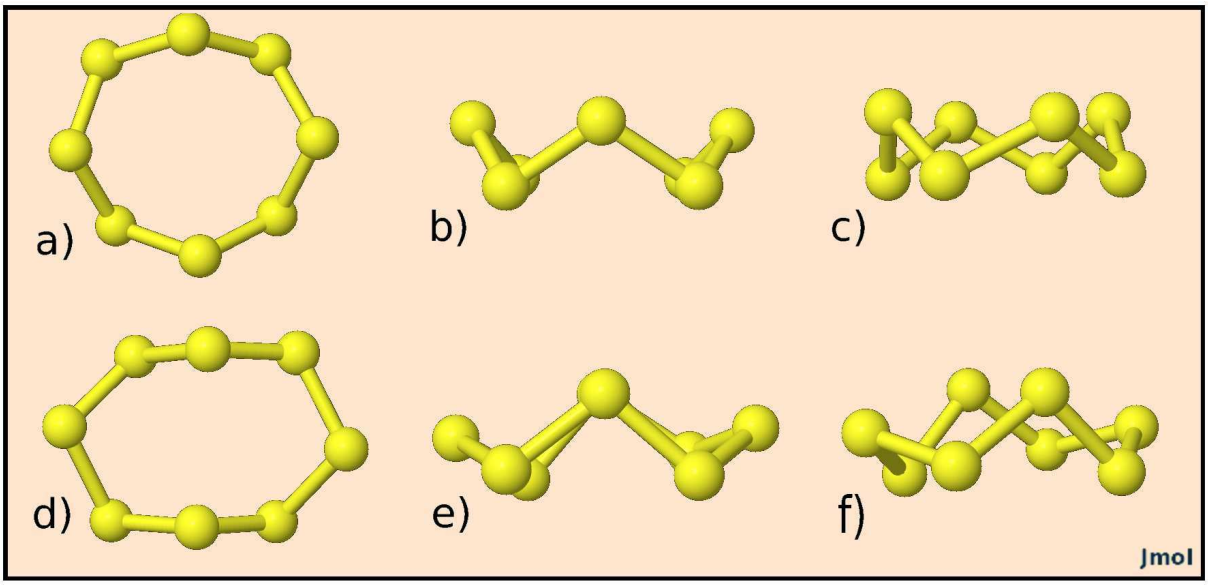

Figure 2: Comparison of type A - a)-c) and type B - d)-f) molecules generated by Jmol. [66]

3.1.2 Simulation methods, results and discussion

To perform most of our *ab initio* MD simulations we used the VASP package [10]. Since VASP does not have implemented any barostat for MD, to simulate system under constant pressure we adopted the idea based on the Berendsen barostat [16] and implemented it to VASP by performing vectors rescaling according to eqs. 14 and 15. The published results were performed on a sample of 512 atoms in a $2 \times 2 \times 1$ supercell of initial S-I structure in a PAW scheme of plane-wave treatment (cutoff 360 eV) of KS orbitals with the PBE GGA functional for XC energy used [6].

We started the simulations from optimized S-I structure at 0 GPa by heating it to room temperature and then started to increase pressure in 10 GPa steps at 300 K. At 20 GPa, we observed a transition into a new molecular phase (denoted m-S) with monoclinic lattice formed by S_8 molecules with two different conformations in the same amount. First molecular type was the most common eight-atomic puckered D_{4d} isomer with shape of crown [58] (type A) and the second originated by deformation of type A to lower C_2 symmetry (type B). Shape of type A and type B molecules is shown in Fig. 2. In order to investigate relative stability of m-S in respect to other crystalline phases, we calculated their EOS of enthalpy over pressure - shown on Fig. 4.

On further pressure increase we observed amorphization at 40 GPa in very good agreement with experiments [32, 55], but we did not observe any significant jump in density that could be associated with the LDA to HDA transition. However, authors of the experiments [55] also admitted possibility that LDA and HDA forms they observed were in facts nanocrystallites. The crystal-to-amorphous form transition at 40 GPa was accompanied by relatively sharp increase of density perhaps indicating a first-order nature of the transition as suggested [55]. Amorphization was also accompanied by metallization.

In order to investigate the PIA mechanism, we focused on tracking the evolution of intra and intermolecular distances before and during PIA. Compression of m-S leads to considerable

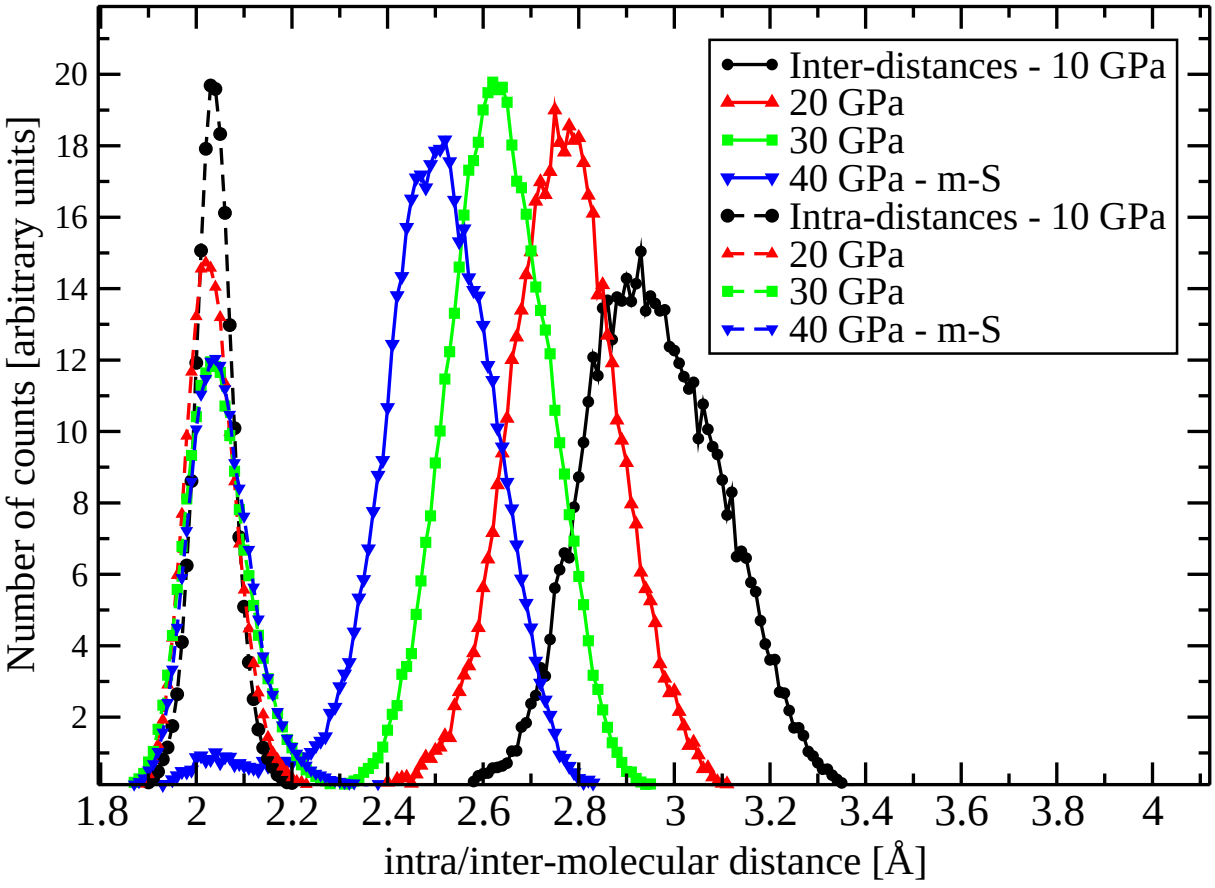

Figure 3: Comparison of bond length and nearest intermolecular distance distributions in S-I at 10 GPa and in m-S at 20-40 GPa. The structure of m-S becomes unstable at 40 GPa, where the two distributions start to overlap. The structure of m-S at 40 GPa contains some bonds between different molecules (defects) that are represented by the small peak around the sulfur covalent diameter of 2.04 Å.

decrease in intermolecular space, while the intramolecular bond lengths remain practically unchanged. In Fig. 3 we show the distributions of the nearest neighbor (n.n.) intramolecular bond lengths and the nearest intermolecular distances in S-I and m-S at pressures from 10 to 40 GPa.

At pressures up to 30 GPa the two distributions are clearly separated and the molecular phase persists. At 40 GPa, the intermolecular distribution develops a small peak located around the sulfur bond length representing the existence of structural defects in m-S, but even without the existence of these defects, the figure reveals that at 40 GPa molecules interact strongly and their intra and interdistance distributions start to overlap. This suggests that PIA is likely to be primarily driven by the overlap of these two distributions, similarly to other cases of molecular to non-molecular transformations in crystals.

In order to further clarify the amorphization transformation, we studed interactions between type A and type B molecules separately from the evolution of the number of intramolecular distances longer than 2.15 Å for A and B molecules separately and of the number of intermolecular distances shorter than 2.2 Å (close intermolecular approachings) for A-A, B-B and A-B pairs separately. We found that type B molecules are more involved in the early stages of amorphization as expected, as far as their intramolecular bond lengths are always somewhat greater than are in A molecules pointing to fact that they are more likely to develop bond breaking. This

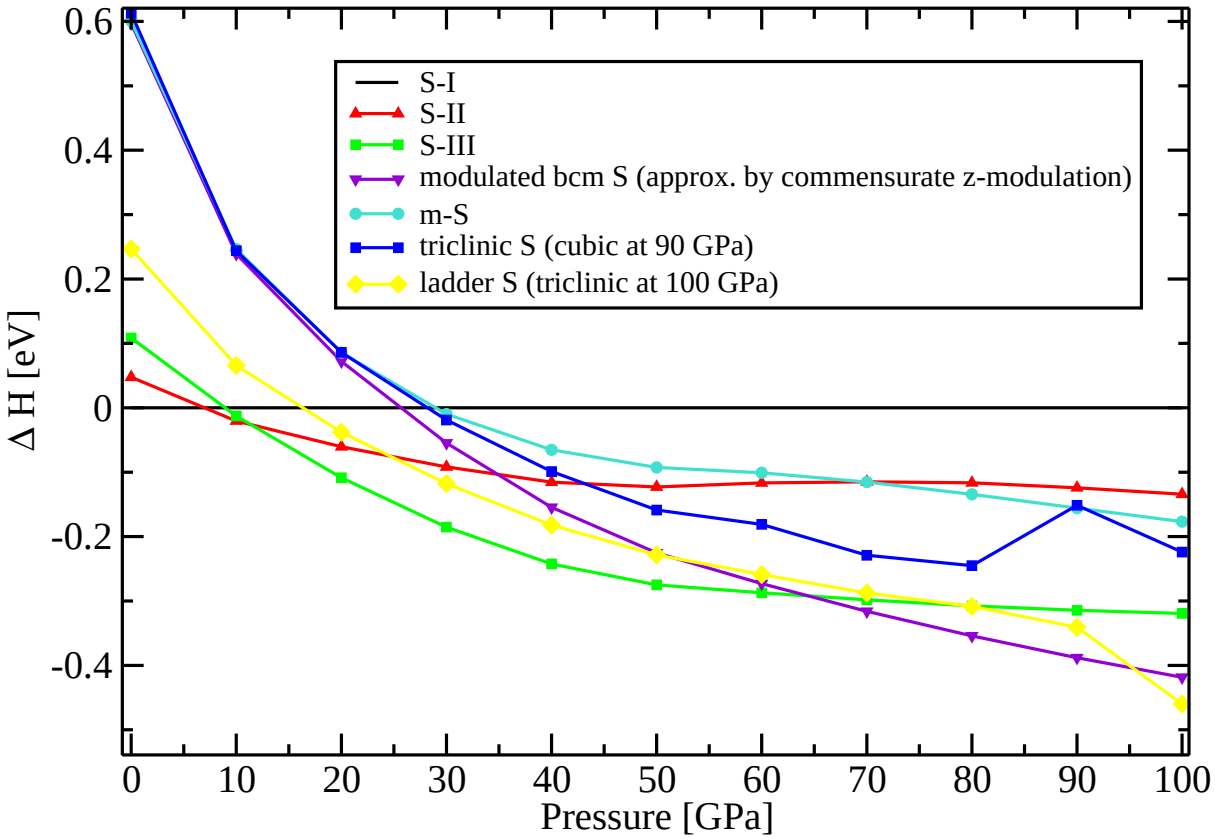

Figure 4: Enthalpies of sulfur phases S-II (red up triangles), S-III (green squares), modulated *bcm* phase S-IV (approximated by commensurate modulation - violet down triangles), m-S (light blue circles), triclinic S (dark blue squares) and ladder S (yellow diamonds) relative to S-I (straight black line) according to calculated EOS. The discontinuities at the endings of the triclinic and ladder curves are caused by structural transformations that took place directly during the optimization algorithm.

is confirmed by recogninition that B-B molecular mixing starts to grow first when amorphization starts. It can be hence concluded that molecular disintegration process is not distributed uniformly between all system components, but the role played by the A and B molecules is different.

Next we analyzed the properties of a-S and its correspondence to the experimental LDA form and to its possible crystalline counterpart. We observed that a-S corresponds quite well to the LDA form [55] according to the resemblance between their RDFs and based on agreement of their densities and also the coordination number N_C. Structural relation of a-S to crystal phase S-III was proposed in the experiment [55] based on the comparison of their density and coordination number and also from the positions of these forms on the phase diagram. Regarding to this problem, we investigated the same properties and concluded that (based on these parameters) our observed a-S could be structurally as well related to it parent phase m-S, and so we cannot state any clear a-S to crystalline phase correspondence.

Minor parts of our simulations were performed by the same methods on smaller sample of 128 atoms (one S-I unit cell) and on the same small sample by CPMD [11]. In both simulations, besides amorphization and m-S structure, we also observed recrystallization of a-S into a simple triclinic structure (one sulfuric atom per cell) which in VASP further transformed to different

"ladder-type" structure. These results have been not published since they need to be confirmed by larger scale simulations.

We performed enthalpy calculations shown in Fig. 4 in order to determine relative stability of the obtained simple triclinic and ladder structures and particularly of the crystalline m-S, in respect to four stable sulfur phases I-IV. We found that m-S is more stable than S-I above 29 GPa and that the triclinic and ladder structures also become more stable than molecular structures at higher pressures. This proves their relative stability and opens a possibility that under certain conditions these two newly predicted phases could be stable.

3.2 Carbon dioxide

Carbon dioxide is very common substance and one of the most important materials found in the Earth's atmosphere and interior, in the Solar system and beyond. It is a dominant component of atmospheres of Mars and Venus and can be found in form of dry ice on surfaces of many other terrestrial objects. High pressure solid CO_2 is very important in geophysics, particularly for it plays an important role in rheological weakening of rocks with consequences for seismic activities and plate tectonics - as new experiments [67] suggested that polymeric CO_2-V can be stable near the top of the lower mantle and then dissociate into diamond and fluid oxygen. Presence of CO_2 in planetary interiors is thereafter important in planetary sciences as it can explain differences in dynamics of the Earth and other planets [68]. Significant amount of polymeric, or even amorphous CO_2 is expected to be present also in deep interiors of giant gaseous planets. Compounds containg amorphous CO_2 are considered for very perspective technological materials for their possible extreme hardness.

3.2.1 Solid phases of CO_2

Thermodynamic phase diagram of CO_2 was a matter of much debate concerning the exact structure and stability of possibly ten distinct crystal phases and the overall consistent picture of CO_2 phases became to emerge only recently based on newest data. Low pressure-temperature solid CO_2 phase I, commonly known as dry ice, is a typical soft molecular solid with linear molecules. This phase transforms into CO_2-III, which is layered with all molecules set in planes. Molecular phase III then upon rising pressure undergoes a chemical reaction associated with sp to sp^3 hybridization, when it transforms to phase V [69, 70], which is fully tetrahedral and metallic.

Though SiO_2 and GeO_2 are prototypes of strong glass-forming materials (either on quenching and compressing), amorphous CO_2 (a-carbonia) is known relatively shortly. First prediction of CO_4 tetrahedra-based amorphous CO_2 came from DFT MD simulations [71] and the first reported observation of a-carbonia suggested existence of mixed three and fourfold-coordinated carbons [72]. More extensive experimental studies [30] reported that amorphization of CO_2-III is preceded by a progressive formation of C-O single bonds and that the amorphous structure seems to be a glassy counterpart of non-molecular phase V. Amorphization of CO_2 at room temperature [73] was proposed to be triggered by close intermolecular approaches reaching minimal sustainable values. The kinetic boundary of amorphization was found to be negatively sloped pointing to kinetical hindrance at low temperatures. It was also noted that this kinetic line

seems to connect to the kinetic boundary of the phase V formation confirming that a-carbonia is most probably amorphous counterpart of phase V. These results were confirmed by *ab initio* MD simulations [74] and also by *ab initio* metadynamics [75]. In addition to PIA, decompressing non-molecular amorphous CO_2 led to transformation into a new molecular amorphous form at 16 GPa [30].

Two important differences between CO_2 and other group IV dioxides include the rigidity of C-O-C intertetrahedral angle (great energy increase on bending out of its well-defined ideal value [76]) and favoring the sp^2 hybridization. The former has important implications for possible structures of CO_2, whereas soft Si-O-Si angle allows silica to form a rich variety of polymorphs, while CO_2 favours only one or two tetrahedral structures. Favoring the sp^2 carbon hybridization results into three-coordinated amorphous form with silica and germanica polymorphs forming always only four or sixfold coordinations.

3.2.2 Preliminary results and discussion

To investigate properties of amorphous CO_2 and mechanism of PIA and to confirm existence of AAT, we adopted basically the same methods and techniques as in the study of sulfur. We performed *ab initio* MD simulations with VASP and Berendsen scheme on relatively small system of 32 CO_2 molecules in a $2 \times 2 \times 2$ extension of CO_2-III unit cell making up simulation supercell. PBE functional of KS DFT and PAW schemes were used with the energy cutoff 450 eV. Currently, we run simulations on much larger and more realistic system of 108 molecules, but the results were not completed in the time of the submission of the PhD thesis.

We started simulations from molecular CO_2-III optimized to 60 GPa and heated to 1000 K when amorphization occurred by progressive creation of three and fourfold-coordinated carbons by nucleation around preceding defects. Decompressing to 10 GPa, the amorphous form changed abruptly from extended amorphous form into a purely molecular amorphous form, in accordance with the experiments [30].

Before the amorphization took place at 60 GPa and 1000 K, we observed creation of structural defects. First defect was created between two parallel planes in the CO_2-III structure and involved three molecules that formed one isolated C≡O carbon monoxide unit and dicarbon pentoxide C_2O_5 object touching the planes. This defective structure then transformed when interpentagonal O-O bond broke and a larger cyclic defect was made out of four adjacent molecules. This C_4O_8 object was also cyclic with a regular sequence of four connected -C-O- units. Shortly after this event, a connection of four different molecules emerged to create chain-C_4O_8. When this highly defective structure started to amorphize, the process was completed practically immediately - within 1.2 ps, during which carbon atoms developed three and four coordinations in a cascade progressing rapidly particularly around the chain defect. The resulting form was amorphous and fully extended in all three dimensions forming three and fourfold-coordinated network. This form is shown on Fig. 6 (left) along the second distinct molecular amorphous form (right). This brief description of the amorphization process is illustrated by evolution of the percentual distribution of carbon coordinations. Each carbon atom can be one-coordinated (monoxide C≡O), two-coordinated (single CO_2 molecule), three (one double and two single bonds) and four-coordinated (four single oxygen bonds) and on Fig. 5, we show the time evolution of this C coordination distribution.

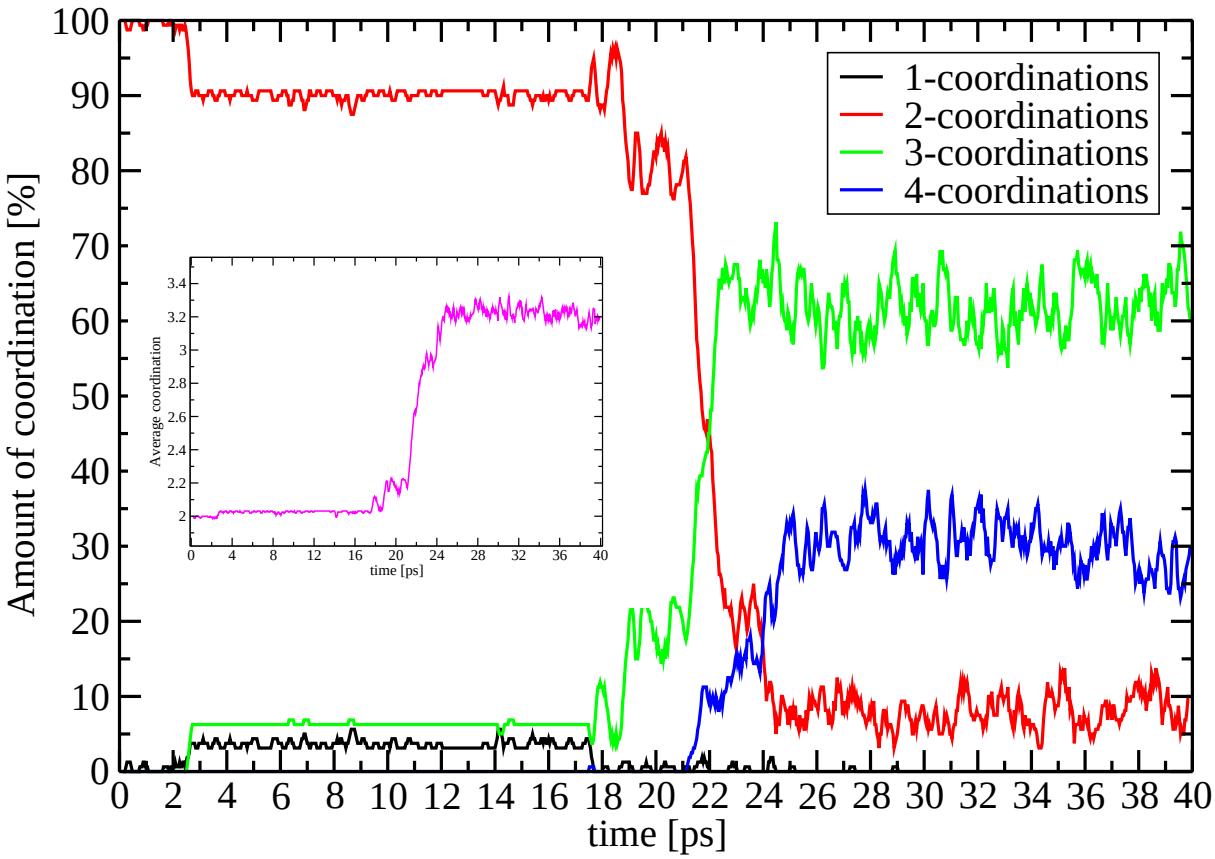

Figure 5: The 40 ps run at 60 GPa and 1000 K. The black (vanishing at 18 ps), red (constantly decreasing from 100%), green (increasing to 70%) and blue (increasing to 30%) curves represent percentual amount of one, two, three and four-coordinated carbons, respectively. The creation of the C_2O_5 pentagon in the 3rd ps, cyclic and chain C_4O_8 objects in the 18th ps and rapid amorphization starting at 21th ps are well visible by sudden changes in the coordination distribution. (Inset) Average carbon coordination at the same time interval throughout the run. The limit for the coordination cutoff was set to 1.5 Å.

From the figure, it can be well seen the creation of all defects and rapid amorphization process represented by extremely quick growth of the three-coordinations (green) and decrease in molecular character (red). In the inset of Fig. 5, the same time evolution is presented for the average carbon coordination starting at the value of 2.0 and ending at value of around 3.2.

At 60 GPa, the mean intermolecular distances in phase III were around 2.3 Å compared to the C=O bond length being around 1.2 Å, and hence we point out that the mechanism of PIA is clearly based on development of structural defects and nucleation of higher pressure phase. This mechanism was definitely favored by relatively high temperatures of our simulations that enabled transition starting before close intermolecular approaches as it was the case of sulfur. Amorphization was found to be very sharp in all properties (with over 12% of inelastic transition volume decrease and energy increase of $\Delta E = 0.18$ eV on one molecule) clearly pointing to a first-order nature of the (non-equilibrium) transition.

The amorphous form at 60 GPa visually appeared similar to tetrahedral structure of non-molecular phase V. We therefore investigated the short-range structure of our simulated a-CO_2 by RDF and ADF distributions and coordination numbers and compared them to phase V α-cristobalite properties. We indeed obtained clear similarities with short-ranged parts of RDFs

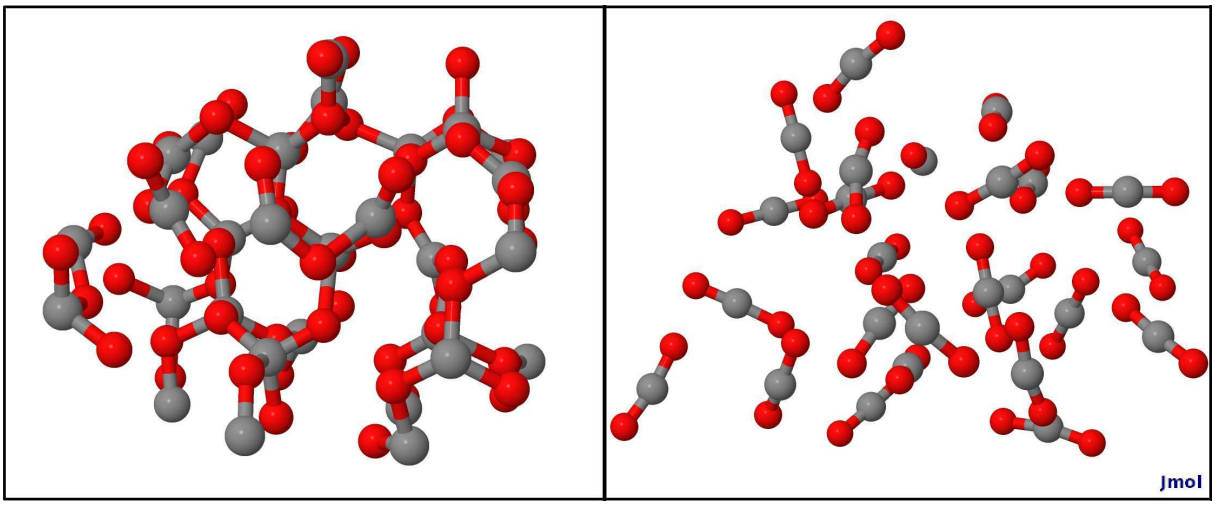

Figure 6: A dramatic example of polyamorphism in CO_2 - two completely different amorphous phases. (Left) Strictly non-molecular (perhaps cristobalite-like) amorphous form of mixed three and fourfold carbon atoms at 60 GPa. (Right) Purely molecular amorphous form formed by linear CO_2 molecules at 10 GPa, pictures by Jmol [66].

and in the values of the coordination numbers N_C with the greatest difference present in N_C of O-O possibly indicating that amorphous carbonia is primary represented by disorder in the oxygen sublattice. The angular distribution of the intertetrahedral C-O-C angle revealed a relatively sharp distribution around the mean value of about 115° and a minor peak around 120°. This is in a good agreement with calculations of "ideal" C-O-C angle in CO_2 crystalline tetrahedral phases estimated to lie between 120-125° [76].

Compression of amorphous CO_2 to 70 and to 80 GPa did not bring any sudden changes in amorphous form and hence we continued with decompression. At 80 GPa, the amorphous form contained roughly the same amount of three and four coordinations, which is in good accordance with other simulations [74, 75] taking into account their P-T history. Decompression from 80 to 20 GPa changed the ratio of three to four-coordinations to the value of 2.44 and the average coordination at 20 GPa was 3.1. At this point, it could be noted that the amorphous forms with great majority of three and fourfold coordinations might be considered as two distinct amorphous forms, but there is most probably no phase transition between them as there is very slow continual change in the 3-4 coordination ratio on de/compression.

On decompression from 20 to 10 GPa, we observed a clear polyamorphic transition in agreement with experiments [30], where such transition was observed at 16 GPa. This new amorphous phase is shown on Fig. 6 (right) along the original extended amorphous form (left). During the quick AAT process, three sudden and very rapid accelerations of the "molecularization" took place and made the entire transition to be finished in a very short time. From clearly large and sudden changes in the structure and physical properties (density and energy), it can be assumed that this polyamorphic transition is also of first-order nature, in strict contrast to gradual changes in non-molecular amorphous CO_2 between intermediate states of different three-to-four coordination ratio value. The new amorphous phase was purely molecular, with linear CO_2 molecules placed randomly in a relatively large space of 35 $Å^3$ on molecule.

4 Summary

In the thesis, we studied nature and mechanism of pressure-induced transformations in solids by means of *ab initio* molecular dynamics simulations at constant high pressure conditions. We aimed at resolving the open questions concerning two interesting and not yet completely understood phenomena of pressure-induced amorphization and amorphous-amorphous transition. We studied two distinct materials with reported amorphization and polyamorphism upon de/compression - elemental sulfur and carbon dioxide. S and CO_2 form very stable molecular crystals at ambient conditions with intramolecular bonds very hard to be broken in order to trigger a transformation. Both compounds thus exhibit large metastability regimes and therefore also the completion of polymorphic transition is kinetically hindered at low temperatures and so once transition starts, crystallization is hindered by a reduced molecular mobility and system remains trapped in some part of amorphous minima megabasin. As far as some of the experimental results were incomplete or controversial, we complemented the experiments by computer modeling, which provides access to information not available from experiments.

Simulations on sulfur were performed mainly on 512 atomic sample and have been published [1], while computations of CO_2 are currently running on 324 atomic sample and were not finished in the time of the thesis submission, hence preliminary results on smaller 96 atomic system were presented. All simulations were performed by VASP[10] and CPMD [11] *ab initio* simulation packages, in case of VASP supplemented by the use of Berendsen barostat [16]. We observed PIA in S and CO_2 in agreement with experiments [55, 30], including amorphization pressures and local structures of the amorphous forms. We did not reproduce AAT in sulfur which can be attributed either to time scale problem of our quantum simulations or to nanocrystalline nature of experimental LDA and HDA forms of sulfur. In case of CO_2, transition from non-molecular amorphous to molecular amorphous form was reproduced very well and agreed with the experimental conditions [30].

We identified the amorphous form of sulfur from our simulations to correspond to the experimentally observed LDA form [55] and amorphous CO_2 from phase III compression contained mixed three and fourfold-coordinated carbons in agreement with the experiments [30, 77, 73] and simulations [74, 75]. Regarding possible relations of amorphous S and CO_2 to underlying crystal phases, we showed that in case of our simulated amorphous sulfur, its short-range structure resembles molecular sulfur, from which it was created as well as the phase S-III, hence leaving this question open. The amorphized phase III of CO_2 shows clear resemblance to phase V cristobalite structure.

Besides the amorphous forms, we also obtained new crystal-crystal polymorphic transitions in sulfur before the onset of amorphization. We denoted the phase as monoclinic sulfur according to change of the lattice symmetry preserving the molecular character. Half of the eight-atomic sulfur molecules changed from original D_{4d} isomers to distorted lower C_2-symmetry isomers. Other crystalline phases of S were observed in smaller system consisting of 128 atoms, namely simple triclinic structure with one atom per unit cell and second structure with regular ladders of sulfur atoms. Calculating enthalpies, we predict these phases might be metastable at certain conditions.

Studying the mechanism of the transitions was one of the major questions we aimed to

resolve. The density-driven amorphization process in sulfur starts at 40 GPa, when the distributions of nearest intra and intermolecular distances begin to overlap. This leads to bond interchanges and eventually to molecular disintegration and formation of structurally disordered phase with different role of original and distorted S_8 molecules played during amorphization. In CO_2, amorphization starts at 60 GPa, when intermolecular distances are slightly lower than twice of the bonds lengths, but before the amorphization, the structure of CO_2-III contains a great portion of defects around which the amorphization clearly progresses. The mechanism of PIA in S and CO_2 thus has similar and also different features. In the case of sulfur, PIA is clearly based on strong molecular overpressurization and considerable shrink of the intermolecular space, while in CO_2 the role of defects seems to be crucial. This can be explained by resistible sulfuric cyclic molecules in respect to linear and open CO_2 ones and also by the fact that CO_2 simulations were performed at higher temperature enabling defects to be created and trigger the transition.

In the case of CO_2, both PIA and AAT transitions occurred relatively sharply and were accompanied by a volume decrease by more than a few %. This probably points to the first-order nature of these transitions, though processing in a non-equilibrium. In the case of sulfur, the associated effects are less clear and do not allow to determine the order of the transition undoubtably.

References

[1] D. Plašienka and R. Martoňák, Phys. Rev. B **85**, 094112 (2012).

[2] M. Born and R. J. Oppenheimer, Ann. Phys. **389**, 457 (1927).

[3] M. C. Payne *et al.*, Rev. Mod. Phys. **64**, 1045 (1992).

[4] P. H. W. Kohn, Phys. Rev. **136**, B864 (1964).

[5] W. Kohn and L. J. Sham, Phys. Rev. **140**, A1133 (1965).

[6] J. P. Perdew, K. Burke, and M. Ernzerhof, Phys. Rev. Lett. **77**, 3865 (1996).

[7] J. Ihm, A. Zunger, and M. L. Cohen, Jour. Phys. C: Solid State Phys. **12**, 4409 (1979).

[8] D. Vanderbilt, Phys. Rev. B **41**, 7892 (1990).

[9] P. E. Blöchl, Phys. Rev. B **50**, 17953 (1994).

[10] G. Kresse and J. Furthmüller, Phys. Rev. B **54**, 11169 (1996).

[11] R. Car and M. Parrinello, Phys. Rev. Lett. **55**, 2471 (1985).

[12] W. C. Swope, H. C. Andersen, P. H. Berens, and K. R. Wilson, Jour. Chem. Phys. **76**, 637 (1982).

[13] S. Gödecker, Jour. Chem. Phys. **120**, 9911 (2004).

[14] A. R. Oganov and C. W. Glass, J. Chem. Phys. **124**, 244704 (2006).

[15] R. Martoňák, Eur. Phys. Jour. B **79**, 241 (2011).

[16] H. J. C. Berendsen *et al.*, J. Chem. Phys. **81**, 3684 (1984).

[17] O. H. Nielsen and R. M. Martin, Phys. Rev. B **32**, 3780 (1985).

[18] A. Laio and M. Parrinello, PNAS **99**, 12562 (2002).

[19] C. A. Angell, Science **267**, 1924 (1984).

[20] F. H. Stillinger and T. A. Weber, Science **225**, 983 (1984).

[21] F. H. Stillinger, Science **267**, 1935 (1995).

[22] P. G. Debenedetti and F. H. Stillinger, Nature **410**, 259 (2001).

[23] M. Goldstein, J. Chem. Phys. **51**, 3728 (1969).

[24] W. Kauzmann, Chem. Rev. **43**, 219 (1948).

[25] L. Berthier and G. Biroli, Rev. Mod. Phys. **83**, 587 (2011).

[26] A. K. Arora, in *High Pressure Phenomena*, edited by R. J. Hemley and G. L. Chiarotti (IOS PRESS, Amsterdam, The Netherlands, 2002), pp. 545–560.

[27] S. M. Sharma and S. K. Sikka, Prog. Mat. Sci. **40**, 1 (1996).

[28] O. Mishima, L. D. Calvert, and E. Whalley, Nature **310**, 939 (1984).

[29] R. J. Hemley *et al.*, Nature **334**, 52 (1988).

[30] M. Santoro *et al.*, Nature **441**, 857 (2006).

[31] S. K. Deb, M. Wilding, M. Somayazulu, and P. F. McMillan, Nature **414**, 528 (2001).

[32] H. Luo and A. L. Ruoff, Phys. Rev. B **48**, 569 (1993).

[33] A. F. Goncharov *et al.*, Phys. Rev. Lett. **85**, 1262 (2000).

[34] T. Yamanaka, T. Nagai, and T. Tsuchiya, Zeit. Krist. **212**, 401 (1997).

[35] M. B. Kruger and R. Jeanloz, Science **249**, 647 (1990).

[36] V. V. Brazhkin *et al.*, Jour. Non-cryst. Solids **212**, 49 (1997).

[37] M. Born, Jour. Chem. Phys. **7**, 591 (1939).

[38] J. S. Tse and D. D. Klug, Phys. Rev. Lett. **67**, 3559 (1991).

[39] J. S. Tse *et al.*, Nature **400**, 647 (1999).

[40] P. F. McMillan, Jour. Mat. Chem. **14**, 1506 (2004).

[41] P. F. McMillan, in *High Pressure Phenomena*, edited by R. J. Hemley and G. L. Chiarotti (IOS PRESS, Amsterdam, The Netherlands, 2002), pp. 511–541.

[42] J. L. Yarger and G. H. Wolf, Science **306**, 820 (2004).

[43] O. Mishima, L. D. Calvert, and E. Whalley, Nature **314**, 76 (1985).

[44] E. Principi *et al.*, Phys. Rev. B **69**, 201201 (2004).

[45] Y. Lin *et al.*, Phys. Rev. Lett. **107**, 175504 (2011).

[46] M. Grimsditch, Phys. Rev. Lett. **52**, 2379 (1984).

[47] J. P. Itie *et al.*, Phys. Rev. Lett. **63**, 398 (1989).

[48] M. Guthrie *et al.*, Phys. Rev. Lett. **93**, 115502 (2004).

[49] J. N. Glosli and F. H. Ree, Phys. Rev. Lett. **82**, 4659 (1999).

[50] Y. Katayama *et al.*, Nature **403**, 170 (2000).

[51] M. Springborg and R. O. Jones, Phys. Rev. Lett. **57**, 1145 (1986).

[52] J. S. Tse and D. D. Klug, Phys. Rev. B **59**, 34 (1999).

[53] T. Loerting and N. Giovambattista, J. Phys.: Condens. Matter **18**, R919 (2006).

[54] D. Daisenberger *et al.*, Phys. Rev. B **75**, 224118 (2007).

[55] C. Sanloup, E. Gregoryanz, O. Degtyareva, and M. Hanfland, Phys. Rev. Lett. **100**, 075701 (2008).

[56] D. Lacks, Phys. Rev. Lett. **84**, 4629 (2000).

[57] K. Trachenko, M. T. Dove, V. Brazhkin, and F. El'kin, Phys. Rev. Lett. **93**, 135502 (2004).

[58] B. Meyer, Chemical Reviews **76**, 367 (1976).

[59] H. Fujihisa *et al.*, Phys. Rev. B **70**, 134106 (2004).

[60] O. Degtyareva *et al.*, Nature materials **4**, 152 (2005).

[61] C. Hejny *et al.*, Phys. Rev. B **71**, 020101 (2005).

[62] S. P. Rudin and A. Y. Liu, Phys. Rev. Lett. **83**, 3049 (1999).

[63] A. Nishikawa, K. Niizeki, and K. Shindo, Phys. stat. sol. (b) **211**, 373 (1999).

[64] E. Gregoryanz *et al.*, Phys. Rev. B **65**, 064504 (2002).

[65] T. Scopigno *et al.*, Phys. Rev. Lett. **99**, 025701 (2007).

[66] Jmol: an open-source Java viewer for chemical structures in 3D. *http://www.jmol.org/.*

[67] K. D. Litasov, A. F. Goncharov, and R. J. Hemley, Earth Planet. Sci. Lett. **309**, 318 (2011).

[68] A. R. Oganov *et al.*, Earth Planet. Sci. Lett. **273**, 38 (2008).

[69] C.-S. Yoo *et al.*, Phys. Rev. Lett. **83**, 5527 (1999).

[70] V. Iota, C.-S. Yoo, and H. Cynn, Science **283**, 1510 (1999).

[71] S. Serra *et al.*, Science **284**, 788 (1999).

[72] C.-S. Yoo, V. Iota, and H. Cynn, Phys. Rev. Lett. **86**, 444 (2001).

[73] T. Kume *et al.*, Jour. Appl. Phys. **102**, 53501 (2007).

[74] J. A. Montoya *et al.*, Phys. Rev. Lett. **100**, 163002 (2008).

[75] J. Sun *et al.*, PNAS **106**, 6077 (2009).

[76] J. Dong, J. K. Tomfohr, and O. F. Sankey, Phys. Rev. B **61**, 5967 (2000).

[77] M. Santoro, J.-F. Lin, H.-K. Mao, and R. J. Hemley, Jour. Chem. Phys. **121**, 2780 (2004).